Four quadrant flux quanta counting for wide-range SQUID amplifiers

Mikko Kiviranta and Nikolai Beev
VTT, Tietotie 3, 02150 Espoo, Finland

E-mail: Mikko.Kiviranta@vtt.fi

Abstract. We have studied flux quanta counting in open loop as a way to implement SQUID amplifiers simultaneously with large dynamic range and small power dissipation. Good signal-to-noise ratio at all flux values is provided by using two SQUIDs, one yielding *sin(ϕ)* and the other *cos(ϕ)* –proportional signal. Lack of feedback in principle lifts the slew rate limitation due to loop causality, present in previously implemented flux quanta counters. Experimental results are shown for up to 180 Φ_0 peak-to-peak flux range with 1.5 $\mu\Phi_0/\mathrm{Hz}^{1/2}$ noise floor, dominated by the digitizer noise. The SQUID and LNA would allow 0.07 $\mu\Phi_0/\mathrm{Hz}^{1/2}$ noise floor with a more silent digitizer. Operation up to 13 Φ_0/μs slew rate was demonstrated, which however is not a fundamental limitation. In our experiment the mismatch between our *sin(ϕ)* and *cos(ϕ)* channels limited the practically achievable slew rate.

1. Introduction

An important figure-of-merit for an amplifier chain is the Shannon capacity [1]

$$C = \Delta f \, \log_2\left(1 + \frac{\phi_{\max}}{\Delta f^{1/2}\,\phi_n}\right) \qquad (1)$$

which can be visualized as the area of a rectangle whose width is the signal bandwidth Δf, and height is the logarithmically plotted dynamic range $D = \phi_{max}/\phi_{n,rms}$. In the case of Direct Current Superconducting Quantum Interface Devices (dc SQUIDs) ϕ_{max} is the maximal tolerated flux signal and $\phi_{n,rms} = \Delta f^{1/2}\,\phi_n$ is the RMS flux noise expressed via the spectral density ϕ_n. Large Shannon capacity is often advantageous, eg. in multiplexed N-pixel systems of cryogenic detectors [2,3] where information flow C_p from each pixel sums into the total flow $N \times C_p$.

Although the thermodynamic nature of amplifiers has been considered before [4] and Landauer's principle is well established [5], the question is open whether copying of a classical bit, or classical amplification process in general, is constrained by some unavoidable entropy production. In practice however, the elements of Shannon capacity of a dc SQUID do seem to be related with heat generation. The heat load becomes important at sub-kelvin temperatures, where every dissipated nanowatt must be lifted to room temperature, and hence be multiplied by inverse efficiency of the refrigerator.

When operated in the standard way within the 0.5 Φ_0 monotonic flux-to-voltage range, the SQUID power dissipation P_d is proportional to the square of the flux dynamic range D [6]. Bandwidth of dc SQUIDs, on the other hand, is limited fundamentally to a fraction of the Josephson frequency ω_J, and in practice limited by resonances of the flux coupling coil [7]. Raising the Josephson frequency leads to an increased voltage $U_{SQ} = 2\pi\omega_J\Phi_0$ across the SQUID, which however does *not* lead to an increased heat generation, if the SQUID current can simultaneously be lowered by making the Josephson junction area smaller. Hence it seems that the heat generation cost of a given Shannon capacity could be lowered by changing the aspect ratio of the Shannon rectangle, i.e. increasing the bandwidth and decreasing the dynamic range. This presumes that there exists a mechanism to trade bandwidth for dynamic range or vice versa.

Negative feedback can be used to increase the dynamic range, either via room temperature as the well-known Flux Locked Loop (FLL) [8] method, or by local feedback [9, 10]. The room temperature version, however, is slew rate limited due to the cable delay and the causality condition of the feedback loop [11]. The locally fed back version, on the other hand, must generate within the cryogenic stage signal power which is by the factor D^2 above the noise floor of the subsequent amplifier stage. Given the power efficiency of the dc SQUID as an

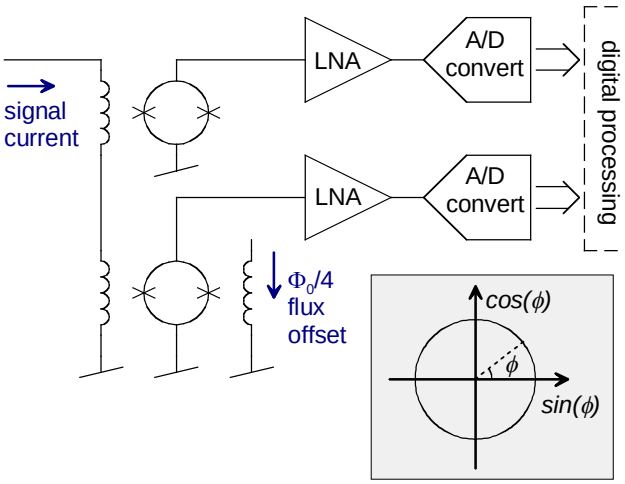

Figure 1: Simplified schematic of the experimental setup, where the first SQUID records the *sin(ϕ)* component and second SQUID the *cos(ϕ)* component of the flux ϕ created by the input signal current. *Inset*: the sin and cos components presented in 2-dimensional space.

amplifier [12], this requirement typically leads to significant heat dissipation.

We propose a technique where dc SQUIDs are operated over several flux quanta, rather than within the 0.5 Φ_0 monotonic flux range. The technique allows one to trade bandwidth for dynamic range, and therefore (i) better match both dynamic range and bandwidth requirements of the particular readout task at hand, and (ii) lower the SQUID heat generation at a given total Shannon capacity prescription. In the technique the signal is read by two SQUIDs (Fig. 1) having a flux offset such that one generates effectively $y(t) = sin(\phi(t))$ and the other $x(t) = cos(\phi(t))$ function of the signal flux $\phi(t)$. With a sufficiently fast digitizer it is possible to take at least three signal samples within one ϕ-vector rotation (inset of Fig. 1), in which case the rotation direction can be determined and the winding number accumulated. The technique is analogous eg. to fringe counting laser interferometers [13] and electromechanical resolvers [14].

Flux quanta counting has been utilized in the past with additional modulation [8], but bandwidth of the approach is limited. Also, integrator reset as part of the ordinary FLL has been utilized [11,15]. Albeit high slew rates have been reached, the technique cannot be scaled further because of the feedback causality condition. Our technique is purely feed forward and not similarly constrained.

Elements other than the SQUID in the signal chain may also act as the dominant dynamic range bottlenecks. Our counting approach alleviates the dynamic range requirement in all subsequent stages, too, at the cost of increased bandwidth. In particular, analog-to-digital converters tend to have larger total

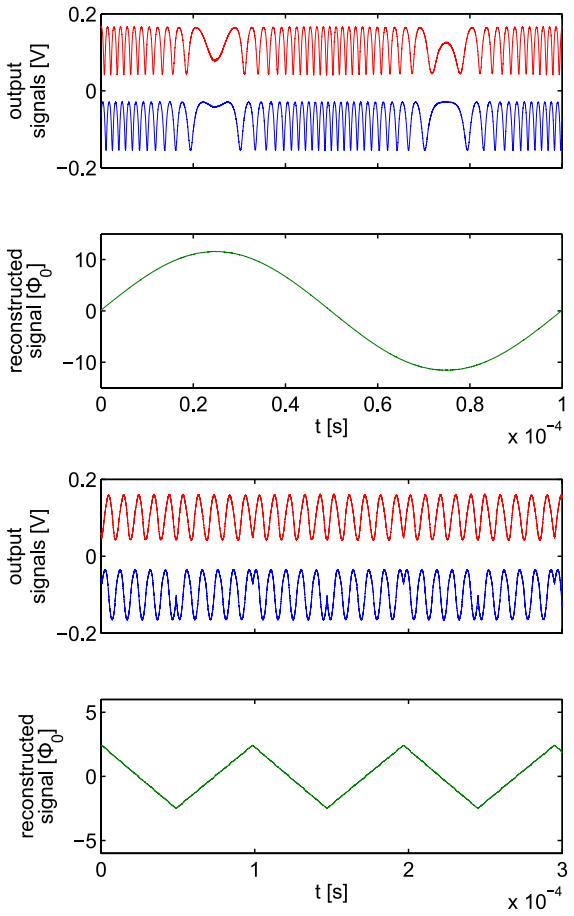

Figure 2: Examples of SQUID output signals, after LNAs, and the reconstructed excitation waveforms. Upper: 10 kHz sinusoid with 20 $\Phi_{0,p\text{-}p}$ amplitude. Lower: 10 kHz triangle wave with 5 $\Phi_{0,p\text{-}p}$ amplitude

Shannon capacity when their dynamic range is small but bandwidth large[1].

2. Experiments

To demonstrate the approach, we have experimented with three different SQUID devices. Device A is a double 60-series 2-parallel array, specifically designed for the sin/cos readout, and fabricated at the side of our standard biomagnetic SQUID [16] test wafer. Device B was constructed by wire bonding together two 60-series SQUID arrays [17] located on the same chip. As device C we used two separate 184-series 4-parallel SQUID array chips [18], with their inputs externally connected in series. The signals from devices A and B were amplified with Drung cell [19] versions of our cryogenic low-

[1] Compare eg. Texas Instruments ADS1675 with 2 MHz Nyquist bandwidth and 93dB SNR implying C = 62 Mbit/s, and ADS5409 with 450 MHz bandwidth and 60 dB SNR implying C = 8900 Mbit/s.

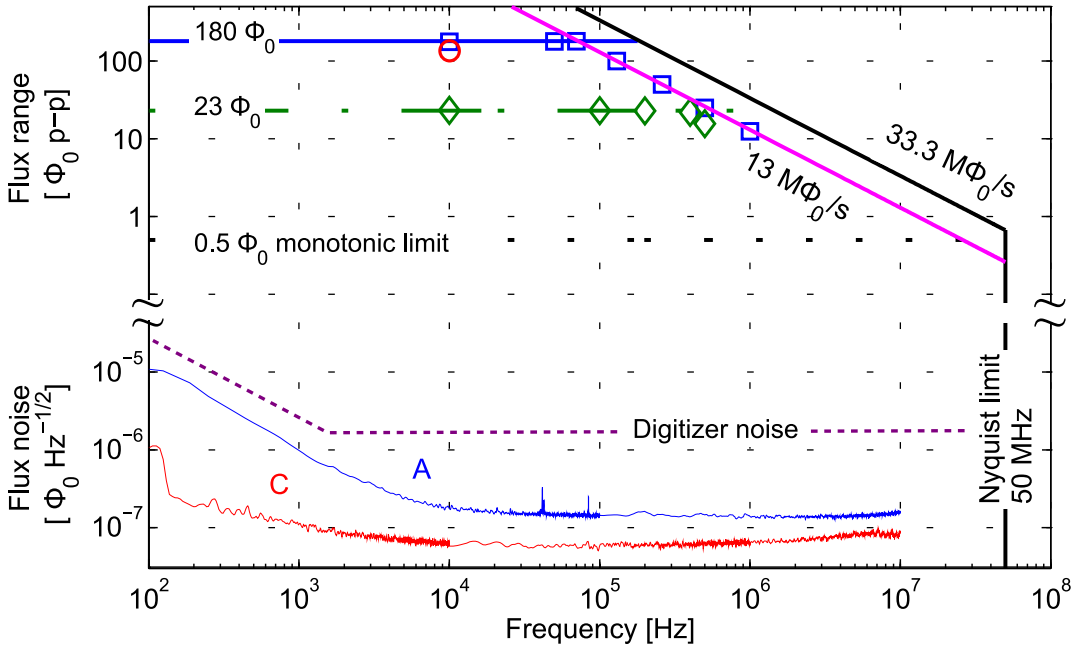

Figure 3: Experimentally recorded and successfully reconstructed amplitude and frequency combinations of sinusoidal excitations with device A (diamonds), device B (squares) and device C (the single circular data point). Also plotted are the flux noise spectra of devices A and C as measured at the LNA outputs with a HP89410A spectrum analyzer. The device B had comparable noise to the device A. Excess noise due to the the Cleverscope digitizer is additionally depicted. Note that noise levels are plotted as 1-Hz spectral densities in the figure, not as the full bandwidt RMS value which appears in the Shannon formula.

noise amplifiers (LNAs) [20]. The Drung cell version has similar noise performance to [20], but dissipates less power owing to the bias current reuse within the first differential transistor pair. The device C was read out by homemade actively terminated room-temperature LNAs built out of discrete SiGe heterojunction transistors. The signals were captured with a two-channel 14-bit 100 MSa/s digitizer [21] and digitally processed. All the experiments were performed at 4.2 K, without superconducting or mu-metal shields.

Full buffers of digitized data were transmitted over Ethernet from digitizer to the host computer, where reconstruction was performed with LabView code. Each order-of 100 kSa sized buffer represented roughly one millisecond worth of data. Although real-time data capture was not attempted, the reconstruction time on the host computer is short enough, order-of millisecond or less, that this appears feasible. Principal value of the reconstructed SQUID phase $\phi(t)$ was obtained by using the four-quadrant inverse tangent, the `atan2(x,y)` function available in LabView. The winding number of $\phi(t)$ can in principle be obtained from a state machine, keeping track whether the quadrants (inset of Fig. 1) are visited clockwise or counter-clockwise. In practical experiments we used the packaged `UnwrapPhase.vi` operation available in LabView.

Examples of signals generated by the two SQUIDs and the reconstructed excitation signals are shown in Fig. 2. The encountered practical limitations are plotted in Fig. 3. Device A began to show flux slipping when the excitation exceeded $\pm 12.5\ \Phi_{0,\text{p-p}}$. We suspect that, because of non-planarized insulation layers, critical current of superconducting lines is exceeded at steps where the line crosses a lower metal edge. In device B, the periodicity of *sin*-generating SQUID is not exactly the same as the periodicity of *cos*-generating SQUID. Due to this, the the mid-excitation 90° phase shift between the SQUIDs degrades to below 60° when flux excursions become larger than $\pm 90\ \Phi_0$. Finally, a Fraunhofer-like modulating envelope [22] over the periodic flux response was observed to reduce the modulation depth of device C at large flux excursions. At $\pm 75\ \Phi_0$ excitation, the modulation depth reduced to 1/3 of its mid-range value. The envelope may be caused by the finite size of the Josephson junctions [22], or by mutual inductance spread within the constituent SQUIDs [23].

The channel-to-channel phase mismatch was, to a smaller extent, present in device C, too, as was the modulation-suppressing envelope in device B. The flux ranges of devices B and C indicated in Fig. 3 are not hard limits, as it was possible to reconstruct the original excitation at even larger flux amplitudes. However, reconstruction fidelity deteriorates rapidly above the limits.

The vertical 50 MHz line in Fig. 3 is the Nyquist limit of our 100 Ms/s digitizer. The 33.3 $\Phi_0/\mu s$ slope indicates the slew rate limitation due to the requirement of at least three samples per rotational cycle. In practice, the slew rate was limited to 13 $\Phi_0/\mu s$ because of poor equalization between the channels. In particular, when the 40 MHz bandwidth of our LNA-dipstick combination [20] is approached, the associated Bode phase shifts become hard to control. The bandwidth was dominated by skin effect of our phosphorus-bronze twisted pairs. These limitations could be relieved with better controlled cabling and a faster digitizer.

Although the 14 bit range over the 50 MHz Nyquist band would imply sufficiently low quantization noise of 10^{-8} $Hz^{-1/2}$ of full scale, we found that there exists significant excess voltage noise of roughly 500 $nV/Hz^{1/2}$ in the digitizer. This limited the practically obtained flux noise floor to 1.5×10^{-6} $\Phi_0/Hz^{1/2}$. To indicate the obtainable performance with a lower-noise digitizer, we included in Fig. 3 the separately measured noise of the SQUID + LNA combinations.

3. Reconstruction fidelity

3.1 Experimental

The range between the signal ceiling and noise floor plotted in Fig. 3 is an indication of the signal-to-noise ratio (SNR) which cannot be improved. There is another more strict limitation, which is not plotted: signal-to-distortion ratio (SINAD), a measure of fidelity of the reconstructed signal. In principle, SINAD can be improved by signal processing techniques, but this often becomes complicated in practice. To get an idea about the fidelity of our reconstruction, we excited device A with a very clean sine wave and studied the distortion in the reconstructed signal. The excitation was generated by a homemade filament-stabilized oscillator [24], measured to have 30 ppm total harmonic distortion. We then attempted to correct the recorded nominally-*sin* and nominally-*cos* signals by the true SQUID flux response shapes, measured quasi-statically over ±0.25 Φ_0 range, and extrapolated over several flux quanta by shifting and mirroring. As an example, when the excitation was ±12.5 $\Phi_{0,p\text{-}p}$ at 10 kHz, we measured -62 dBc and -73 dBc second harmonic and -76 dBc and -89 dBc third harmonic levels, respectively without and with the numerical correction. The meagre improvement suggests that correction by the static half-period of the SQUID response is too simple a technique, as it does not take into account other fidelity-degrading mechanisms (see below).

3.2 Discussion

Practically obtainable reconstruction fidelity is a complicated question. Some static imperfections, i.e. effects which do not depend on the rate of change of the signal, are collected in the Table 1. These effects are deterministic, and can in principle be calibrated out, at least partially. The Table 1 shows uncorrected numbers. The $\varepsilon = 0.001$ periodicity mismatch is comparable to our B device, and $\gamma_S = \gamma_C = 0.005$ suppression comparable to our C device.

The modulation-suppressing envelope, to the extent it is caused by mutual inductance spread [23], can be alleviated by using single SQUIDs rather than arrays. The Fraunhofer-like part of the envelope is caused by finite size of Josephson junctions relative to the loop perimeter [22], and can be alleviated by designing larger SQUID loops. Our B and C devices were off-the-shelf arrays, whose SQUID loops are moderately small, and therefore not optimal for wide flux ranges. Periodicity mismatch depends on fractional accuracy of the geometric SQUID dimensions, which, too, would improve in larger-loop SQUID designs.

The dominant *dynamic* imperfection is the finite bandwidth of the LNA and the readout chain. Realistic treatment of the problem would involve the readout transfer function, only constrained by Bode causality relations [25], and then convoluted with the well-known [26] series expansion of the SQUID output signals. Such treatment is beyond the scope of the paper at hand. A qualitative rule-of-thumb can be given, however, that the flux signal whose slew rate nowhere exceeds x Φ_0/s, does not generate higher SQUID output frequency components than $1/x$. Conversely, a readout chain with brick-wall transfer function, with f_0 corner frequency and perfectly matched phase behaviour, would pass without degradation any flux signal whose slew rate nowhere exceeds $f_0\times\Phi_0$. In practice, phase matching would be complicated, because Bode relations imply a broad transition in phase response when the amplitude response is sharp (brick-wall).

Further complication arises when noise is taken into account, and determination of SNR is

Table 1: Examples of numerically calculated fractional error $\delta_\phi = \max\left|\phi_{REC} - \phi\right| / \phi_{MAX}$ when the reconstructed flux is $\phi_{REC} = \arctan(y/x) + 2\pi \times$ winding number.

Static non-ideality type		$\phi/2\pi$ = 0…10 Φ_0	$\phi/2\pi$ = 0…100 Φ_0
Periodicity mismatch $y = \sin((1+\varepsilon)\phi)$ $x = \cos((1-\varepsilon)\phi)$	ε = 0.001	δ_ϕ = 0.001	δ_ϕ = 0.0013
	$\varepsilon = 1\times10^{-4}$	$\delta_\phi = 1\times10^{-4}$	$\delta_\phi = 1\times10^{-4}$
Suppressed modulation $y = \sin(\phi)/(1+\gamma_S\lvert\phi\rvert)$ $x = \cos(\phi)/(1+\gamma_C\lvert\phi\rvert)$	Symmetric $\gamma_S = \gamma_C$	In absence of noise $\delta_\phi = 0$	
	γ_S = 0.005 γ_C = 0	δ_ϕ = 0.002	δ_ϕ = 0.001
Non-sinusoidal response $y = \sin\phi + a_2\sin^2\phi + a_3\sin^3\phi + \ldots$ $x = \cos\phi + b_2\cos^2\phi + b_3\cos^3\phi + \ldots$	Symmetric $a_2 = b_2$ = - 0.8 $a_3 = b_3$ = + 0.3	δ_ϕ = 0.008	$\delta_\phi = 8\times10^{-4}$

attempted. For example, suppressed SQUID modulation depth does not affect reconstruction fidelity if suppression occurs symmetrically in both sin- and cos- quadratures, but it does increase the relative effect of the LNA noise and hence degrades the SNR. When static, dynamic and noise-related effects are present in the system simultaneously, and their interplay is significant, there probably is not an easier approach than full computer simulation for estimating the reconstruction fidelity.

4. Conclusion

The four-quadrant flux counting method is a promising way to reach extremely high slew rates, unhindered by fundamental limitations such as feedback loop causality. For better practical results, more attention will be needed for the channel-to-channel equalization, digitizer speed and digitizer noise. SQUIDs specifically designed for wider Fraunhofer envelopes and well matched flux periodicities would be helpful, too. Reconstruction fidelity could be improved by addition of local negative feedback, in which case the SQUID responses would resemble two sawtooth waves, with flux offset between them.

An attractive improvement would be addition of a third ‘coarse’ channel [27], which could resolve the flux count number, without the need for the digitizer to keep track of the vector rotation. The two ‘fine’ channels would then be needed only to provide a constant signal-to-noise ratio at all flux values within one period.

We find the flux-counting approach valuable in wide-range readout applications such as high-resolution magnetometry in earth’s field [27] or magnetoencephalography [28] with relaxed magnetic shielding. Our primary application will be amplification of the summed signal from several multiplexed X-ray TES calorimeters, particularly in the Code Domain multiplexed [3] configuration, where there are no easy ways to increase the SQUID dynamic range without intolerable increase in power dissipation.

Acknowledgement

This work was supported in part by the E-SQUID project, grant no. 262947 of the European Communitys 7th framework programme (FP7/2007-2013). Partial support was received from the Center of Excellence in Low Temperature Quantum Phenomena and Devices, Academy of Finland.

References

[1] Cover T M and Thomas J A 2006 Elements of information theory, *Wiley series in telecommunications and signal processing* Ch 10.3.
[2] Kiviranta M, Seppä H, van der Kuur J and de Korte P 2002 SQUID-based readout schemes for microcalorimeter arrays *AIP Conf. Proc.* **605** 295-300.
[3] Irwin K D et al 2012 Advanced code-division multiplexers for superconducting detector arrays *J Low Temp Phys* **167** 588-94.
[4] Scovil H E D and Schulz-DuBois E O 1959 Three level masers as heat engines *Phys. Rev. Lett.* **2** 262-3.
[5] Landauer R 1991 Information is physical *Physics Today* **44** (5) 23-9.
[6] Kiviranta M et al 2003Dc and un SQUIDs for readout of ac-biased transition edge sensors *IEEE Tran. Appl. Supercond.* **13** 614-7.

[7] Mück M et al 1999 Microstrip superconducting quantum interference device radio-frequency amplifier: tuning and cascading *Appl. Phys. Lett.* **75** 3545-7.
[8] Forgacs R L and Warnick A 1967 Digital-Analog Magnetometer Utilizing Superconducting Sensor *Rev. Sci. Instr.* **38** 214-220.
[9] Irwin K D and Huber M E 2001 SQUID operational amplifier *IEEE Tran. Appl. Supercond.* **11** 1265-70.
[10] Kiviranta M 2006 Use of SiGe bipolar transistors for cryogenic readout of SQUIDs *SuST* **19** 1297-302.
[11] Drung D 2003 High-Tc and low-Tc dc SQUID electronics *SuST* **16** 1320-36.
[12] Kiviranta M 2012 Amplifier development for multiplexed cryogenic detectors *J. Phys. Conf. Series* **400** 052014.
[13] Rowley W R C 1966 Some aspects of fringe counting in laser interferometers *IEEE Tran. Instr. Meas.* **15** 146-9.
[14] Bell J and Langham E M 1951 Mean-wind-velocity instruments for use on naval craft *Proc. IEE – Part II: Power Engineering* **98** 448-52.
[15] Ludwig C, Kessler C, Steinfort A J and Ludwig W 2001 Versatile High Performance Digital SQUID Electronics *IEEE Tran. Appl. Supercond.* **11** 1122-5.
[16] Penttilä J, Grönberg L, Hassel J and Kiviranta M 2009 Optimized SQUID sensors for low frequency measurements *J. Phys. Conf. Series* **150** 052209 (4pp).
[17] Kiviranta M, Grönberg L and Hassel J 2012 A Multiloop SQUID and a SQUID Array With 1-µm and Submicrometer Input Coils *IEEE Tran. Appl. Supercond.* **22** 1600105 (5 pp).
[18] Kiviranta M, Grönberg L, Beev N and van der Kuur J 2014 Some phenomena due to SQUID input properties when local feedback is present *J. Phys. Conf. Series*, in press.
[19] Drung D, Storm J-H and Beyer J 2013 SQUID current sensor with differential output *IEEE Tran. Appl. Supercond.* **23** 1100204 (4pp).
[20] Beev N and Kiviranta M 2013 Fully differential cryogenic transistor amplifier *Cryogenics* **57** 129-33.
[21] Cleverscope CS328A-XSE, http://www.cleverscope.com
[22] Jaklevic R C et. al. 1965 Macroscopic quantum interference in superconductors *Phys. Rev.* **140** A1628-37.
[23] Häussler Ch, Oppenländer J and Schopohl N 2001 Nonperiodic flux to voltage conversion of series arrays of dc SQUIDs *J. Appl. Phys.* **89** 1875-9.
[24] Williams J 1990 Bridge circuits *Linear Technology application note 43.*
[25] Bode H W 1945 *Network analysis and feedback amplifier design.* D. van Nostrand publishing company.
[26] Abramowitz M and Stegun IA 1970 *Handbook of mathematical functions*, equations 9.1.42 and 9.1.43 .
[27] Schönau T et al 2013 SQUID-based setup for the absolute measurement of the Earth's magnetic field *SuST* **26** 035013 (7pp).
[28] Hämäläinen M et al 1993 Magnetoencephalography — theory, instrumentation, and applications to noninvasive studies of the working human brain interference *Rev. Mod. Phys.* **65** 413-97.